Biallelic pathogenic variants in roundabout guidance receptor 1 associate with syndromic congenital anomalies of the kidney and urinary tract

Johannes Münch[1,2,31], Marie Engesser[2,31], Ria Schönauer[1,2], J. Austin Hamm[3], Christin Hartig[2], Elena Hantmann[1,2], Gulsen Akay[4,5], Davut Pehlivan[4,6,7], Tadahiro Mitani[4], Zeynep Coban Akdemir[4,8], Beyhan Tüysüz[9], Toshihiko Shirakawa[10], Sumito Dateki[11], Laura R. Claus[12], Albertien M. van Eerde[12], Genomics England Research Consortium[13], Thomas Smol[14], Louise Devisme[15], Hélène Franquet[15], Tania Attié-Bitach[16,17], Timo Wagner[18], Carsten Bergmann[18,19], Anne Kathrin Höhn[20], Shirlee Shril[21], Ari Pollack[22], Tara Wenger[22], Abbey A. Scott[23], Sarah Paolucci[24], Jillian Buchan[24], George C. Gabriel[25], Jennifer E. Posey[4], James R. Lupski[4,7,26], Florence Petit[27], Andrew A. McCarthy[28], Gregory J. Pazour[29], Cecilia W. Lo[25,32], Bernt Popp[30,32] and Jan Halbritter[1,2,32]

[1]*Department of Nephrology and Medical Intensive Care, Charité-Universitätsmedizin Berlin, Berlin, Germany;* [2]*Division of Nephrology, University of Leipzig Medical Center, Leipzig, Germany;* [3]*East Tennessee Children's Hospital, Genetic Center, Knoxville, Tennessee, USA;* [4]*Department of Molecular and Human Genetics, Baylor College of Medicine, Houston, Texas, USA;* [5]*Department of Pediatrics, University of Utah, Salt Lake, Utah, USA;* [6]*Division of Neurology and Developmental Neuroscience, Department of Pediatrics, Baylor College of Medicine, Houston, Texas, USA;* [7]*Texas Children's Hospital, Houston, Texas, USA;* [8]*Department of Epidemiology, Human Genetics, and Environmental Sciences, Human Genetics Center, School of Public Health, University of Texas Health Science Center at Houston, Houston, Texas, USA;* [9]*Department of Pediatric Genetics, Istanbul University Cerrahpasa Medical Faculty, Istanbul, Turkey;* [10]*Department of Pediatrics, Nagasaki University Hospital, Nagasaki, Japan;* [11]*Department of Pediatrics, Nagasaki University Graduate School of Biomedical Sciences, Nagasaki, Japan;* [12]*Department of Genetics, University Medical Center Utrecht, Utrecht, the Netherlands;* [13]*Genomics England Research Consortium (GEL) - 100,000 Genomes Project, London, UK;* [14]*Centre Hospitalier Universitaire de Lille, Institut de Génétique Médicale, Lille, France;* [15]*Centre Hospitalier Universitaire de Lille, Institut de Pathologie, Lille, France;* [16]*Laboratoire de biologie médicale multisites SeqOIA, Paris, France;* [17]*Service de Médecine Génomique des Maladies Rares, APHP.Centre, Université de Paris, Paris, France;* [18]*Medizinische Genetik Mainz, Limbach Genetics, Mainz, Germany;* [19]*Department of Medicine, Nephrology, University Hospital Freiburg, Freiburg, Germany;* [20]*Division of Pathology, University of Leipzig Medical Center, Leipzig, Germany;* [21]*Division of Nephrology, Boston Children's Hospital, Boston, USA;* [22]*Division of Genetic Medicine, University of Washington, Seattle, Washington, USA;* [23]*Division of Genetic Medicine, Seattle Children's Hospital, Seattle, Washington, USA;* [24]*Department of Laboratory Medicine and Pathology, University of Washington, Seattle, Washington, USA;* [25]*Department of Developmental Biology, University of Pittsburgh School of Medicine, Pittsburgh, Pennsylvania, USA;* [26]*Department of Pediatrics, Baylor College of Medicine, Houston, Texas, USA;* [27]*Centre Hospitalier Universitaire de Lille, Clinique de Génétique Guy Fontaine, Lille, France;* [28]*European Molecular Biology Laboratory, Grenoble, France;* [29]*Program in Molecular Medicine, University of Massachusetts Medical School, Biotech II, Worcester, USA; and* [30]*Institute for Human Genetics, University of Leipzig Medical Center, Leipzig, Germany*

Congenital anomalies of the kidney and urinary tract (CAKUT) represent the most common cause of chronic kidney failure in children. Despite growing knowledge of the genetic causes of CAKUT, the majority of cases remain etiologically unsolved. Genetic alterations in roundabout guidance receptor 1 (ROBO1) have been associated with neuronal and cardiac developmental defects in living individuals. Although Slit-Robo signaling is pivotal for kidney development, diagnostic *ROBO1* variants have not been reported in viable CAKUT to date. By next-generation-sequencing methods, we identified six unrelated individuals and two non-viable fetuses with biallelic truncating or combined missense and truncating variants in *ROBO1*. Kidney and genitourinary manifestation included unilateral or bilateral kidney agenesis, vesicoureteral junction obstruction, vesicoureteral reflux, posterior urethral valve, genital malformation, and increased kidney echogenicity. Further clinical characteristics were remarkably heterogeneous, including neurodevelopmental defects, intellectual impairment, cerebral malformations, eye anomalies, and cardiac defects. By *in silico* analysis, we determined the functional significance of identified missense variants and observed absence of kidney ROBO1

Correspondence: *Cecilia W. Lo, Department of Developmental Biology, University of Pittsburgh School of Medicine, Clinical Translational Science Institute, 530 45th Street, 8120 Rangos Research Center, Pittsburgh, Pennsylvania 15201, USA. E-mail: cel36@pitt.edu; or Bernt Popp, Institute of Human Genetics, University of Leipzig Medical Center, Philipp-Rosenthal-Street 55, 04103 Leipzig, Germany. E-mail: bernt.popp@medizin.uni.leipzig.de; or Jan Halbritter, Department of Nephrology and Medical Intensive Care, Charité - Universitätsmedizin Berlin, Charitéplatz 1, 10117 Berlin, Germany. E-mail: jan.halbritter@charite.de*

[31]These authors contributed equally to this work.

[32]Equally contributing corresponding authors.

Received 24 February 2021; revised 30 November 2021; accepted 11 January 2022; published online 26 February 2022

expression in both human and murine mutant tissues. While its expression in multiple tissues may explain heterogeneous organ involvement, variability of the kidney disease suggests gene dosage effects due to a combination of null alleles with mild hypomorphic alleles. Thus, comprehensive genetic analysis in CAKUT should include *ROBO1* as a new cause of recessively inherited disease. Hence, in patients with already established *ROBO1*-associated cardiac or neuronal disorders, screening for kidney involvement is indicated.

Kidney International (2022) **101,** 1039–1053; https://doi.org/10.1016/j.kint.2022.01.028

KEYWORDS: CAKUT; dysplastic kidneys; ROBO1; Slit-Robo signaling; VUR

Congenital anomalies of the kidney and urinary tract (CAKUT) affect approximately 1% of all live births and represent the predominant cause of pediatric chronic kidney failure.[1] CAKUT also contribute to end-stage kidney disease in adults, especially when early diagnosis was overlooked during infancy.[2] The congenital nature of CAKUT, its frequent syndromic presentation, and familial clustering, each suggest a strong genetic basis for this condition. Indeed, more than 50 genes have been characterized to play a role in CAKUT to date.[3,4] Alterations in these genes, however, collectively only explain approximately 20% of cases.[4,5] Unraveling CAKUT etiologies is further complicated by genetic and phenotypic heterogeneity, incomplete penetrance, and complex genetics.[4,5] Recently, a genome-wide analysis of copy number variations[6] delineated major associated genetic signals, and studies suggest a gene dosage effect with expression below haploinsufficiency levels during kidney development.[7]

CAKUT subsumes dysregulated kidney morphogenesis, leading to various kidney malformations including bilateral or unilateral renal agenesis and hypoplasia, multiplex/duplex kidneys, multicystic dysplastic kidneys, ureteropelvic junction obstruction, ureterovesical junction obstruction, vesicoureteral reflux (VUR), and posterior urethral valve disorders.[8] This vast spectrum illustrates the challenges in timely identification of all patients, as both severe and mild clinical courses exist. CAKUT can occur isolated or as part of a syndrome. Depending on the underlying molecular mechanism, involvement of multiple tissues and organ systems is common.[9] In syndromic CAKUT, concomitant chronic kidney disease (CKD) may not necessarily represent the predominant clinical issue but requires nephrologists' and urologists' care in order to at best avoid or at least manage complications.

In this study, we report 6 unrelated individuals from families with sporadic disease and 1 family with 3 fetuses, all of which suffer from syndromic CAKUT associated with biallelic variants in *ROBO1* (Mendelian Inheritance in Man [MIM], *602430).

Roundabout guidance receptors (ROBOs) constitute a highly conserved subfamily of immunoglobulin superfamily proteins characterized by a single-pass transmembrane domain and interaction with the soluble extracellular Slit ligands.[10] *ROBO1*, which was originally identified in a *Drosophila* mutant screen, was shown to be crucial for proper axon guidance and neocortical development.[11] Later, *ROBO1* was shown to be involved in non-neuronal developmental processes, such as those of the lung, heart,[12] muscle, limbs,[13] and angiogenesis including the kidney.[11,14,15] Molecular genetics of *ROBO1*, however, remained somewhat elusive, as both monoallelic[12,16,17] and anecdotal cases of biallelic mutations[18–20] were reported without evolving into a clearly associated phenotype. Heterozygous *ROBO1* variants were predominantly reported in patients with congenital heart disease[12] and neurodevelopmental disorders, such as pituitary stalk interruption syndrome.[16,17] However, genetic association with genitourinary tract malformation is limited to the report on a family with repetitive fetal demise and bilateral renal agenesis[19] and indications from rare variant burden analysis.[21] In contrast, for the *ROBO1* paralog *ROBO2*,[22,23] and in other genes being implicated in Slit-Robo signaling such as *SLIT2*[24] and *SRGAP1*,[24] putatively disease-causing variants were detected in various families with CAKUT.[24] Therefore, this study aims to answer the question whether genetic alterations of *ROBO1* contribute to disturbed kidney development and to further characterize the impact of *ROBO1* variants on renal and extrarenal phenotypes.

METHODS

Written informed consent was obtained from all participants and their parents included in this study, approved by the local institutional review board (IRB) at the Universities of Leipzig (Germany; IRB00001750; #402/16-ek), Nagasaki (Japan), Istanbul (Turkey; with written informed consent for participation in Baylor College of Medicine IRB-approved protocol H-29697 for research exome sequencing), the East Tennessee Children's Hospital (USA), the Seattle Children's Hospital (USA), from the Genomics England 100,000 Genome Project (REC reference 14/EE/1112), and from the France Genomic Medicine Plan 2025. Genetic analysis was conducted from blood-derived DNA or fetal lung samples by either exome sequencing (ID 2, ID 3, ID 4, ID 5, ID 6), whole genome sequencing (ID 7), or next-generation sequencing-based gene panel analysis comprising all 426 CKD-associated genes (ID 1; Supplementary File S1). Direct sequencing (Sanger dideoxy nucleotide sequencing) was used for variant confirmation by orthogonal DNA sequencing strategy and for segregation analysis whenever affected relatives (ID 8, ID 9) or parental samples were available. RNA extraction from blood lymphocytes was performed with the PAXgene blood system (Becton Dickinson), followed by cDNA synthesis using the SuperScript II Reverse Transcriptase Kit (Invitrogen). Obtained cDNA was subsequently analyzed by reverse transcription–polymerase chain reaction and Sanger sequencing for differentiation of the variant's origin. Consecutive employment of the *GeneMatcher* platform,[25] literature research, and unbiased variant filtering of the 100,000 Genomes Project, managed by *Genomics England*, were used for the identification of additional cases with biallelic *ROBO1* variants. Additional phenotypic data were collected by structured clinical questionnaires sent to the corresponding physicians of each patient.

Protein linear structure with corresponding domains was visualized with missense constraint scores based on *Uniprot Q9Y6N7*. Tertiary protein structure models were generated through the *GalaxyDom*/*GalaxyTBM* pipeline[26,27] and visualized using PyMOL (Schrödinger).

An N-ethyl-N-nitrosourea (ENU)–induced mouse model of *Robo1*, harboring the homozygous missense mutation Ile207Thr (NM_019413.2), was previously published.[12,28] Paraffin-embedded sections were dewaxed and rehydrated. Sections for immunofluorescence were autoclaved for 45 minutes in 10 mM citrate buffer pH 6 before staining. Antibodies used include T1α (DSHB clone 8.1.1), acetylated tubulin (Sigma 611-B1), and gamma tubulin (Sigma GTU88). Kidney segments were marked with fluorescein isothiocyanate–labeled Dolichos biflorus agglutinin and Lotus tetragonolobus agglutinin. For endogenous ROBO1 staining in murine and human kidney sections, we performed immunohistochemistry with an anti-ROBO1 antibody (600-401-692S). Specificity of the anti-ROBO1 antibody (600-401-692S; 1:100) was validated *in vitro* by costaining in HeLa cells that were transiently transfected with eYFP-tagged ROBO1 plasmids (500 ng, Lipo2000).

RESULTS

Clinical characteristics and genetic analysis

The 44-year-old index patient (ID 1) was genetically evaluated for chronic kidney failure of unknown etiology while awaiting kidney transplantation.[2] As an infant, he suffered from repetitive pyelonephritis due to VUR caused by unilateral ureterovesical junction obstruction and a posterior urethral valve requiring surgical intervention within his first year of life. Nevertheless, renal function stabilized over the years until a slowly progressive decrease in function led to bilateral atrophic kidneys and end-stage kidney disease at the age of 44 (Figure 1a). Extrarenally, he presented with bilateral strabismus (Figure 1b) and mitral valve prolapse (Figure 1c; Supplementary Movies SV1A and SV1B). Motor and cognitive skills developed normally. On gene panel analysis of 462 known and candidate CKD genes (Supplementary Table S1), this individual was found to carry 2 rare heterozygous likely damaging *ROBO1* variants (Figure 1d, Table 1): 1 missense (NM_002941.3: c.818T>C, p.(Val273Ala)) and 1 truncating variant (NM_002941.3: c.1198C>T, p.(Gln400*)). In the absence of paternal DNA, we confirmed compound heterozygosity by maternal segregation analysis and reverse transcription–polymerase chain reaction, indicating nonsense-mediated RNA decay of the truncating allele and exclusive expression of the missense allele yielding "apparent homozygosity" of the identified variant (Figure 1d). Subsequent retrospective central nervous system–phenotyping by cerebral magnetic resonance imaging showed no marked anomalies except for a missing "bright spot" at the posterior pituitary gland (Figure 1e).

In search of additional individuals with biallelic *ROBO1* variants and a shared CAKUT phenotype, we employed the *GeneMatcher* platform,[25] undertook retrospective phenotyping in previously published cases with biallelic *ROBO1* alterations, and searched for patients with biallelic *ROBO1* variants with at least 1 truncating variant within the 100,000 Genomes Project dataset. As a result, we identified another 5 families with 1 affected individual each and 1 family with 3 affected fetal cases, 2 of whom displayed renal in addition to extrarenal phenotypes, compatible with syndromic CAKUT.

In contrast to the index patient, additional cases were pediatric, aged 0–8 years, originating from Japan (ID 2), Turkey (ID 3), the USA (ID 4, ID 5), and the UK (ID 6), or fetal cases, from 17 to 26 weeks of gestation (WG) originating from France (ID 7, ID 8); the pediatric ascertainment may more reflect potential syndromic CAKUT than chronic kidney failure in the adult subject.

First, ID 2, the previously published case of an 8-year-old Japanese boy with hereditary pituitary malformation, came to our attention for the identified homozygous splice site variant c.1342+1G>A affecting the canonical splice donor of exon 10 of *ROBO1* (NM_002941.3).[20] As kidney phenotypes were beyond the scope of the initial report, we retrospectively evaluated him for urorenal involvement and did obtain information on increased bilateral renal echogenicity (Figure 1), slightly reduced kidney size, impaired kidney function (CKD stage G2), and hypogonadism with micropenis, the latter being likely related to hypopituitarism and/or hypospadias. Furthermore, the patient's growth rate was reduced, and his general appearance included dysmorphic features together with intellectual disability, psychomotor delay, sensorineural hearing loss, and strabismus. Morphologically, nervous system anomalies comprised thinning of the corpus callosum and hypoplasia of the pons and midbrain (Table 1).

Second, patient 3 (ID 3), an unpublished case of a 5-year-old boy from Turkey, was first evaluated at 3 years of age. Urorenal manifestation encompassed bilateral renal hyperechogenicity, slightly reduced kidney size, and bilateral cryptorchidism. Again, body height ranged in the 3rd–10th percentile and dysmorphic features, intellectual impairment, psychomotor delay, eye anomalies (bilateral strabismus, atrophic iris), and dextrocardia were part of the clinical syndrome associated with another homozygous splice site variant at c.2882+1G>T affecting the canonical splice donor of exon 21 and predicted to undergo nonsense mediated decay[29] (NM_002941.3; Figure 1, Table 1). Notably, his craniofacial features (Figure 1i) strongly resemble that of ID 2,[20] with frontal bossing, bitemporal narrowing, medially upslanting eyebrows, and low set, posteriorly rotated ears. His neurodevelopmental phenotype was also striking for the observation of mirror hand movement disorder. No likely damaging variants in *DCC* or *RAD51*, previously associated with autosomal dominant mirror movements (MIM #157600, 614508), were identified by exome sequencing. Brain magnetic resonance imaging revealed lateral ventricle widening secondary to supratentorial white matter volume loss, corpus callosum splenium agenesis, a small thalamus, and atrophic changes at the mesencephalopontine level, findings overlapping those observed in ID 2.[20]

Third, patient 4 (ID 4), a 2-year-old Caucasian girl from the United States, manifested congenitally when an abdominal ultrasound revealed left-sided renal agenesis (Figure 1l

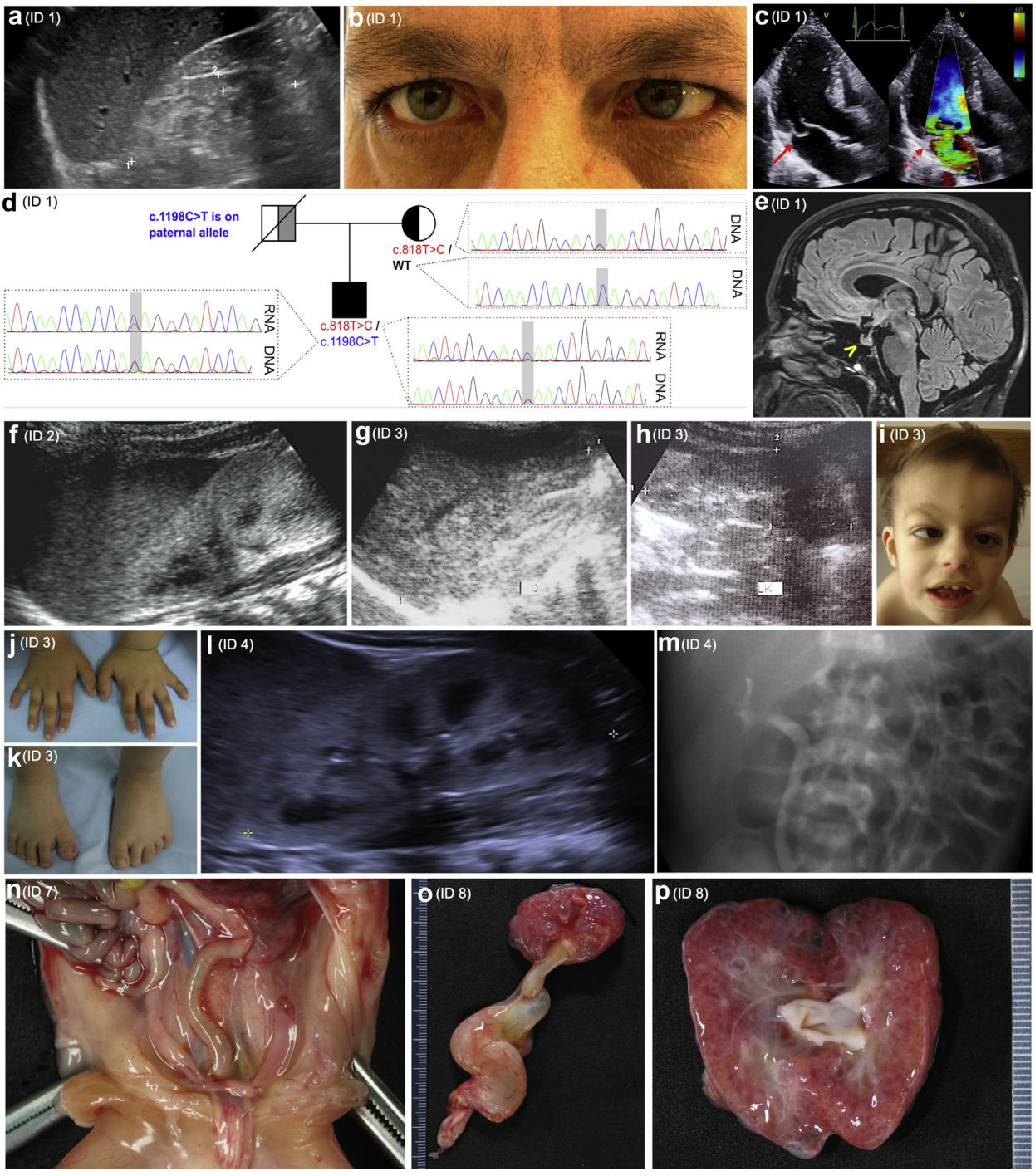

Figure 1 | Renal and extrarenal phenotypes of individuals with biallelic *ROBO1* variants. Index patient ID 1 (**a**–**e**). (**a**) Abdominal ultrasound shows an atrophic right kidney that is hardly definable from the surrounding tissue (length 8.6 cm; parenchyma 0.8 cm). The left kidney (not shown) is atrophic as well. The parenchyma of the right kidney has a singular small cyst. (**b**) Strabismus of the left eye at the age of 44. Of note, the patient had already undergone corrective surgery for this eye malposition during adolescence. (**c**) Transthoracic echocardiography shows a mild-to-moderate mitral valve regurgitation due to primary P2-mitral valve prolapse of the posterior leaflet (red arrow, left side) with an anterior directed jet formation (red dotted arrow, right side) in the apical long axis view (Supplementary Movies SV1A and SV1B). (**d**) Segregation analysis in the mother of ID 1 showed the missense variant c.818T>C, p.(Val273Ala) (NM_002941.3) and excluded the nonsense variant in her c.1198C>T, p.(Gln400*) (NM_002941.3) (upper-right box). The father was deceased and thus not available for segregation analysis. To confirm that the nonsense variant lies on the paternal allele, we performed reverse transcription–polymerase chain reaction on RNA derived from peripheral blood lymphocytes of individual ID 1 with 2 exon spanning primer pairs covering the 2 variants, respectively. Sanger sequencing of cDNA showed a reduced expression of the allele with the nonsense variant c.1198C>T, p.(Gln400*), which is expected to be degraded through nonsense-mediated RNA decay (lower-left box). Contrary the maternal variant c.818T>C, p.(Val273Ala) showed monoallelic expression (lower-right box). Together these results demonstrate that the 2 variants are in trans (comp.-het.). However, our analysis cannot differentiate whether the nonsense variant was inherited from the father or arose *de novo* on the paternal allele. (Continued)

and m). In addition, grade 3 VUR, mild hydronephrosis, and increased renal echogenicity with cystic dysplasia were observed on the right kidney (Figure 1l). Similar to previous cases, this patient displayed a reduced growth rate and also showed dysmorphic facial features, psychomotor delay, and a patent foramen ovale. Unfortunately, there was no clinical information regarding nervous system or eye anomalies. Analogous to ID 1, exome sequencing yielded 2 novel heterozygous *ROBO1* variants, a truncating (NM_002941.3: c.2924G>A, p.(Trp975*)) and a missense variant (NM_002941.3: c.2065T>C, p.(Ser689Pro)) that segregated among nonconsanguineous parents in accordance with Mendelian expectations (Table 1).

Fourth, patient 5 (ID 5), a 10-year-old boy from nonconsanguineous parents of Mexican descent, manifested congenitally with unilateral renal agenesis, cardiac anomalies (including tetralogy of Fallot and pulmonary artery stenosis), and severe central nervous system malformations (including agenesis of the corpus callosum). He also has other anomalies, including intellectual disability, global developmental delays, mixed hearing loss, and subglottic stenosis requiring tracheostomy. On trio exome sequencing, the following compound heterozygous truncating variants in *ROBO1* were identified (NM_002941.3): c.687C>G, p.(Tyr229*); c.2758C>T, (p.Arg920*) (Table 1). This patient inherited his *ROBO1* c.687C>G, p.(Tyr229*) variant from his mother and the *ROBO1* c.2758C>T, p.(Arg920*) variant from his father.

For unbiased replication of associated phenotypes and in order to estimate the frequency of deleterious biallelic *ROBO1* cases, we searched 78,195 germline genomes of participants from the 100,000 Genomes Project (aggV2 v11—GRCh38) for additional instances of biallelic *ROBO1* alterations. Filtering criteria included at least 1 truncating variant, minor allele frequency <0.001, and a CADD_PHRED score >20 (or no Combined Annotation Dependent Depletion [CADD] score if not applicable).[30] By applying these criteria, we identified 1 individual (ID 6) carrying compound heterozygous truncating variants in *ROBO1* (NM_002941.3: c.850G>T, p.(Glu284*); c.4156G>T, p.(Gly1386*)). Interestingly, this female infant also exhibited unilateral renal agenesis, dysmorphic facial features, and intellectual impairment, similar to ID 5 (Table 1).

Lastly, we describe a previously unreported family with 3 affected fetal cases (ID 7, ID 8, and ID 9) from France. The parents are healthy and nonconsanguineous (Caucasian mother and African father) and have 2 healthy children. ID 7 was a female fetus whose pregnancy was terminated at 17 WG after antenatal diagnosis of increased nuchal translucency at first trimester, anamnios, and bilateral kidney agenesis associated with ventriculomegaly. Fetal examination confirmed the bilateral kidney agenesis with Potter sequence (Figure 1n) and revealed a left hemiuterus with right ovarian agenesis, premature ossification of the sternum, and multiple cerebral anomalies (aqueductal stenosis with hydrocephalus, partial agenesis of the corpus callosum, vermis hypoplasia, absence of pyramidal tracts, and dentate nuclei hypoplasia). ID 8 was a male fetus whose pregnancy was terminated at 22 WG after antenatal diagnosis of anamnios, left kidney agenesis, and large right polycystic kidney (Figure 1o and p), associated with enlarged cerebral ventricles and vermis hypoplasia. Fetal examination revealed an obstruction of the right ureterovesical junction responsible for the kidney dysplasia (Figure 1o). CAKUT was associated with facial dysmorphism (large eyebrows, anteverted nares), club-feet, short and large hands, premature ossification of the sternum, and multiple cerebral anomalies (enlarged ventricles, vermis hypoplasia, absence of pyramidal tracts, and dentate nuclei hypoplasia). ID 9 was a male fetus whose pregnancy was terminated at 26 WG after antenatal diagnosis of lymphedema of the first trimester, heart defect, and ventriculomegaly. Fetal examination revealed facial dysmorphism (large eyebrows, anteverted nares and bulbous nose, and micrognathia), left heart hypoplasia with pulmonary atresia and ventricular septal defect, absence of ductus arteriosus, abnormal lung segmentation (4 lobes on the right side), and premature ossification of the sternum and multiple cerebral anomalies (enlarged ventricles, partial agenesis of the corpus callosum, absence of pyramidal tracts, and dentate nuclei hypoplasia). However, no CAKUT was identified in this case. On trio whole genome sequencing with DNA samples from ID 7 and from both parents, the following compound heterozygous truncating variants in *ROBO1* were identified in ID 7 (NM_002941.3): c.2630_2631del; p.(Pro877Argfs*4); c.4015_4018del; p.(Ala1339Argfs*31) (Table 1). Variant c.4015_4018del; p.(Ala1339Argfs*31) was inherited from his father and variant c.2630_2631del; p.(Pro877Argfs*4) from his mother. By Sanger sequencing both *ROBO1* variants subsequently segregated in ID 8 and ID 9.

In summary, except for the first missense variant c.818T>C, p.(Val273Ala), all identified *ROBO1* changes were novel, and hence were absent from both population databases (gnomAD[31]) and patient databases (ClinVar/HGMD-

Figure 1 | (Continued) (**e**) Cerebral magnetic resonance imaging (MRI) revealed a missing "bright spot" of the posterior pituitary gland (sagittal, T1-weighted MRI; yellow arrowhead indicates the pituitary gland). Patient ID 2 (picture **f**). (**f**) Both kidneys show an increased echogenicity at 2 months of age. Sonography at the age of 8 years revealed a kidney size of 7.4 × 2.9 cm (right) and 7.7 × 2.6 cm (left, not shown). Patient ID 3 (pictures **g**–**k**). At the age of 5 years, both kidneys show an increased echogenicity. (**g**) Right kidney (size 7.2 × 3.1 cm). (**h**) Left kidney (size 7.6 × 2.6 cm). (**i**) Facial features demonstrate frontal bossing, bitemporal narrowing, strabismus, medially upslanting eyebrows, bulbous tip of nose, and low set, posteriorly rotated ears. (**j**) Hand examination is notable for brachydactyly and bilateral fifth finger clinodactyly. (**k**) Feet are notable for brachydactyly and increased spacing between the first and second digits. Patient ID 4 (pictures: **l**, **m**). (**l**) Abdominal ultrasound shows an increased echogenicity of the singular right kidney (length 6.8 cm) at the age of 2 years. (**m**) Postpartum, the patient had vesicoureteral reflux into the right kidney which was resolved at 2 years of age. Patient ID 7-8 (pictures: **n**–**p**) (**n**) Bilateral renal agenesis at 17 weeks of gestation in ID 7. (**o**) Obstruction of the right ureterovesical junction responsible for dilated ureter and unilateral polycystic kidney dysplasia at 22 weeks of gestation (ID 8). (**p**) Right polycystic kidney dysplasia with missing corticomedullar differentiation at 22 weeks of gestation (ID 8).

Table 1 | Genetic and clinical summary of the *ROBO1* cohort

Patient	ID 1	ID 2	ID 3	ID 4	ID 5	ID 6	ID 7	ID 8
ROBO1 variant	comp. het.	hom.	hom.	comp. het.	comp. het.	comp. het.	comp. het.	
First allele—c. position	c.818T>C	c.1342+1G>A	c.2882+1G>T	c.2065T>C	c.687C>G	c.850G>T	c.2630_2631del	
First allele—p. position	p.(Val273Ala)	*Splice site*	*Splice site*	p.(Ser689Pro)	p.(Tyr229*)	p.(Glu284*)	p.(Pro877Argfs*4)	
Allele frequency (gnomAD)	0.04%	Not listed	Not listed	Not listed	Not listed	Not listed	Not listed	
Second allele—c. position	c.1198C>T	c.1342+1G>A	c.2882+1G>T	c.2924G>A	c.2758C>T	c.4156G>T	c.4015_4018del	
Second allele—p. position	p.(Gln400*)	*Splice site*	*Splice site*	p.(Trp975*)	p.(Arg920*)	p.(Gly1386*)	p.(Ala1339Argfs*31)	
Allele frequency (gnomAD)	Not listed	Not listed	Not listed	Not listed	Not listed	Not listed	Not listed	
Sex	Male	Male	Male	Female	Male	Female	Female	Male
Origin	Germany (Caucasian)	Japan (Asian)	Turkey (Caucasian)	US (Caucasian)	US (Mexican)	UK (Caucasian)	France (Caucasian, African)	
Parental consanguinity	–	+	+	–	–	–	–	
Age at inclusion	44 yr	8 yr	5 yr	2 yr	10 yr	0–4 yr	17 WG	22 WG
Age at first manifestation	1 yr	Postnatal	3 yr	Congenital	Congenital	Congenital	Antenatal	Antenatal
Renal manifestation								
Chronic kidney disease (stage)[a]	G5 Age at ESKD: 44 yr	G2	G1	G2	G2 Note: renal biopsy showed FSGS	NA	NA	Polycystic kidney
Vesicoureteral reflux	+	–	–	+	–	NA	NA	NA
Ureterovesical junction obstruction	+	–	–	–	–	–	NA	+
Posterior urethral valve	+	–	–	–	–	–	–	–
Increased echogenicity	+	+ Slightly reduced kidney size	+ Slightly reduced kidney size	+	+	NA	NA	–
Renal agenesis	–	–	–	Unilateral	Unilateral	Unilateral	Bilateral	Unilateral
Genital malformation	–	Micropenis	Cryptorchidism	–	–	–	Hemiuterus, unilateral ovarian agenesis	–
Extrarenal manifestation								
Decreased growth rate	–	+	+	–	+	NA[b]	–	–
Body height (percentile)	Normal	Decreased (<3rd at 18 mo)	Decreased (3rd–10th)	Normal (50th)	Decreased (3rd)	NA[b]	Normal	Normal
Dysmorphic facial features	–	+	+	+	+	+	+	+
Intellectual impairment	–	+	+	NA	+	+	NA	NA
Psychomotor delay	–	+	+	+	+	NA[b]	NA	NA
Pituitary gland anomaly	+	+	–	–	–	NA[b]		–
Eye anomalies	Strabismus, hyperopia	Strabismus	Strabismus, atrophic iris	NA	Hypertelorism	NA[b]	–	–

(*Continued on following page*)

Table 1 | (Continued) Genetic and clinical summary of the *ROBO1* cohort

Heart anomalies	Mitral valve prolapse	–	Dextrocardia	PFO	TOF with PS, WPW	NA[b]	–	–
Other			Mirror hand movement		Subglottic stenosis, agenesis of the corpus callosum, mixed hearing loss	NA[b]	Aqueductal stenosis with hydrocephalus, partial agenesis of corpus callosum, vermis hypoplasia, pyramidal tracts, and dentate nuclei agenesis	Ventriculomegaly, vermis hypoplasia, pyramidal tracts agenesis, dentate nuclei hypoplasia, and clubfeet

cm, centimeter; comp. het., compound heterozygous; ESKD, end-stage kidney disease; FSGS, focal segmental glomerulosclerosis; hom., homozygous; mo, months; NA, not applicable; PFO, patent foramen ovale; PS, pulmonary stenosis; TOF, tetralogy of Fallot; WG, weeks of gestation; WPW, Wolff-Parkinson-White syndrome.
[a]Chronic kidney disease refers to the classification of the Kidney Disease: Improving Global Outcomes (KDIGO) initiative. gnomAD v2.1.1—population-specific allele frequency (http://gnomad.broadinstitute.org/).
[b]Detailed data unavailable due to policy of the 100,000 Genomes Project.
The variants reported refer to RefSeq NM_002941.3.

Professional Version 2021.3). Only the Val273Ala change was present in gnomAD, reported heterozygously in 0.04% of cases from European non-Finnish origin, compatible with a rare hypomorphic allele without incidences of homozygosity in the gnomAD database. The 2 patients with homozygous *ROBO1* alterations (ID 2 and ID 3) were born to consanguineous parents (Table 1), and their variants probably arose from identity-by-descent under an hypothesis of a Clan Genomics model rather than represent a founder allele.[32,33] Notably, the variant identified in ID 3 (c.2882+1G>T), which is positioned within a 534.4 Mb region of absence of heterozygosity (AOH) within the proband, is not present in either a heterozygous or homozygous state in any other individual in a local (Baylor-Hopkins Center for Mendelian Genomics [BHCMG]) Turkish database of 952 subjects, supporting the rarity of this variant within the Turkish population. Similarly, the variant identified in ID 2 (c.1342+1G>A) is not present in either a heterozygous or homozygous state in TogoVar (https://togovar.biosciencedbc.jp), a database of genomic variants from 4700 Japanese individuals.

In silico variant prediction

ROBO1 is a 180 kDa receptor protein with a single helical transmembrane domain.[34] The extracellular portion, responsible for homodimerization and Slit-ligand binding, contains 5 well-defined N-terminal Ig-like domains followed by 3 fibronectin type III (FN3) domains. In contrast, the unstructured C-terminal tail represents a nonspecified cytoplasmic region (Figure 2a). All 12 *ROBO1* variants reported in our study were single-nucleotide substitutions: 2 canonical splice site variants, 8 truncating variants, and 2 missense variants, the latter 2 located within the functionally important Ig and FN3 protein domains (Figure 2a). The functional importance of these extracellular domains is further underscored by continuously higher CADD scores (approximately 25) compared with the unstructured C-terminus (Figure 2b). Both amino acid substitutions (p.(Val273Ala): CADD_PHRED_v1.6 = 25.9; p.(Ser689Pro): CADD_PHRED_v1.6 = 27.4) involve evolutionarily conserved residues, on multiple sequence alignment (MSA) of Ig- and FN3-domains across human ROBO1-4 paralogs (Figure 2c and d; Supplementary Figures S1 and S2) and various species orthologs (Figure 2e and f; Supplementary Figures S3–S6). In order to further assess identified missense variants for their predicted impact on 3-dimensional protein architecture, we performed homology modeling based on the recently published ROBO2 crystal structures[34] and analyzed this together with another recently published pseudo-atomic dimer-of-dimers model of Robo1 (Figure 3a–d; Supplementary Figure S7).[35–37] Our homology model shows high structural similarity with both previously reported models, which together support different folding states at the transition between Ig-4/Ig-5 (longer linker) and FN3-1/FN3-2 (compare Figure 2a and Supplementary Figure S8). We thereby mapped p.(Val273Ala) (ID 1) on the

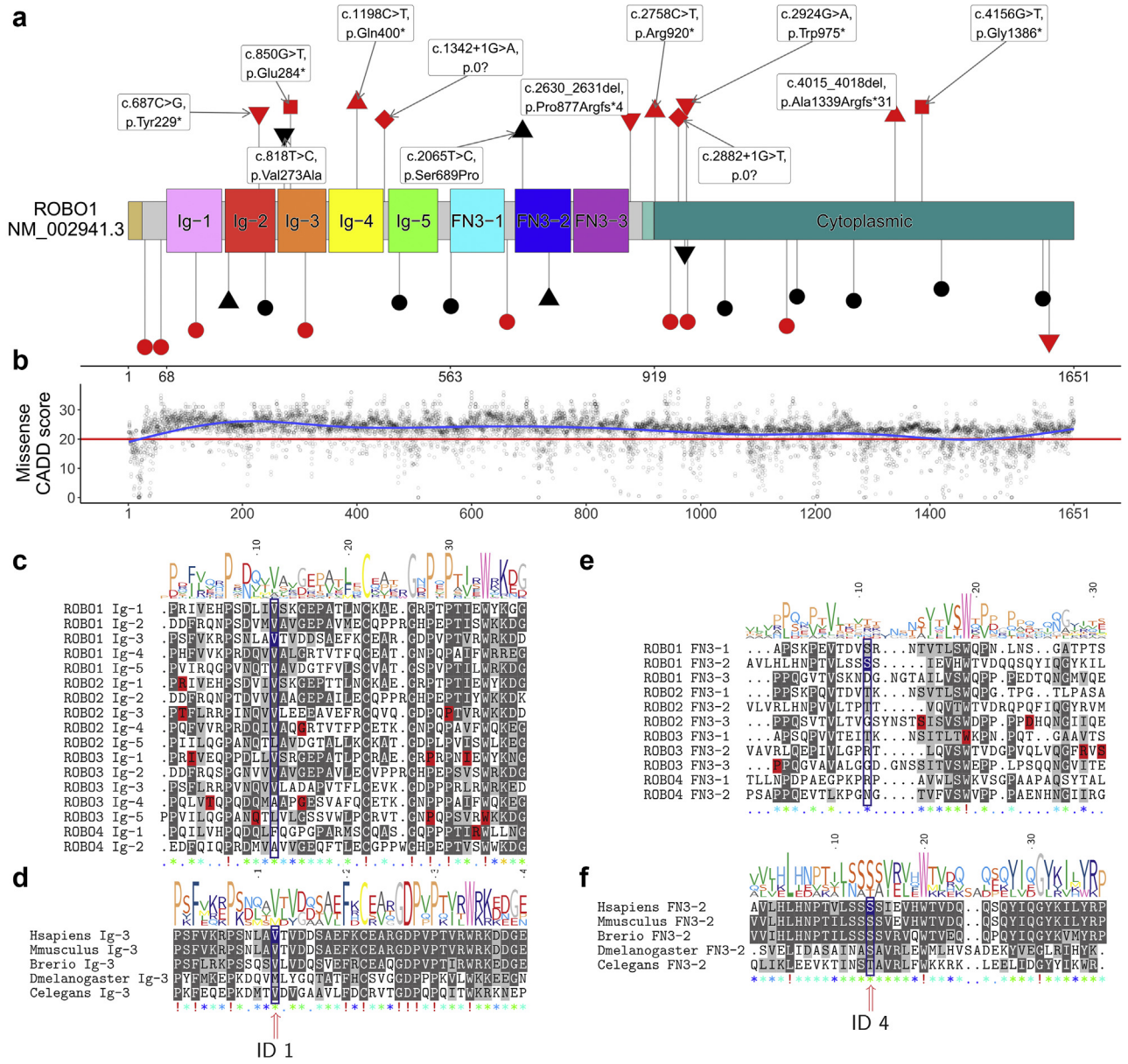

Figure 2 | ROBO1 domain structure with variant distribution and sequence conservation. (**a**) Schematic of the ROBO1 protein (based on Uniprot Q9Y6N7) with 5 Ig-like C2-type (Ig-1 to Ig-5) and 3 fibronectin type III (FN3-1 to FN3-3) domains in the extracellular protein part (AA positions 26-872) colored according to the schematic used by Barak *et al.*[34] The N-terminal signal peptide is colored in gold, the helical transmembrane domain in light green, and the unstructured C-terminal cytoplasmic domain is colored in dark green. Disease-associated *ROBO1* variants identified in the cohort (ID 1–ID 6) are depicted above the schematic; variants described in the literature for different disorders are shown below the schematic (red: truncating, black: missense, rhomb: homozygous, circle: heterozygous, triangle down: compound-heterozygous maternal, triangle up: compound-heterozygous paternal, segment length: CADD score). The missense variants c.818T>C, p.(Val273Ala) (ID 1) and c.2065T>C, p.(Ser689Pro) (ID 4) affect the Ig-3 and FN3-2 domains, respectively. (**b**) The blue lines shows smoothed CADD values for all possible missense variants in ROBO1 across the linear protein structure and the red horizontal line indicates the recommended cutoff for this computational score.[30] This plot indicates that the ROBO1 protein (especially the extracellular domain containing the Ig and FN3 domains) is highly conserved. (**c**) Multiple-sequence alignment (MSA) of all Ig domains of ROBO1 orthologs shows high sequence conservation at the missense variant position c.818T>C, p.(Val273Ala) (ID 1; marked in blue and indicated with a red arrow) and indicates that the valine at this position is important across different Ig domains and orthologs. Red shading indicates positions at which missense variants have been described as associated with disease in the respective ROBO protein. Gray shading represents conservation, and a sequence conservation logo is presented above the alignment (only AAs 1-60 shown, see also Supplementary Figure S1 and Supplementary File S2 sheet "Related_variants"). (**d**) The MSA for the Ig-3 domain in ROBO1 paralogs (AAs 1-65) shows high evolutionary conservation at the positions of missense variants identified in ID 1(compare Supplementary Figures S3 and S4). (**e**) MSA for all FN3 domains of ROBO1 (AAs 1-40) shows that the missense variant position c.2065T>C, p.(Ser689Pro) ID 4 is conserved only in FN3-1/FN3-2 of ROBO1 and thus likely has subtype-specific function (compare Supplementary Figure S2). (**f**) The MSA for ROBO1 paralogs (AAs 1-40) shows high evolutionary conservation of the FN3-2 domain (F; compare Supplementary Figures S5 and S6) at the positions with a missense variant in ID 4.

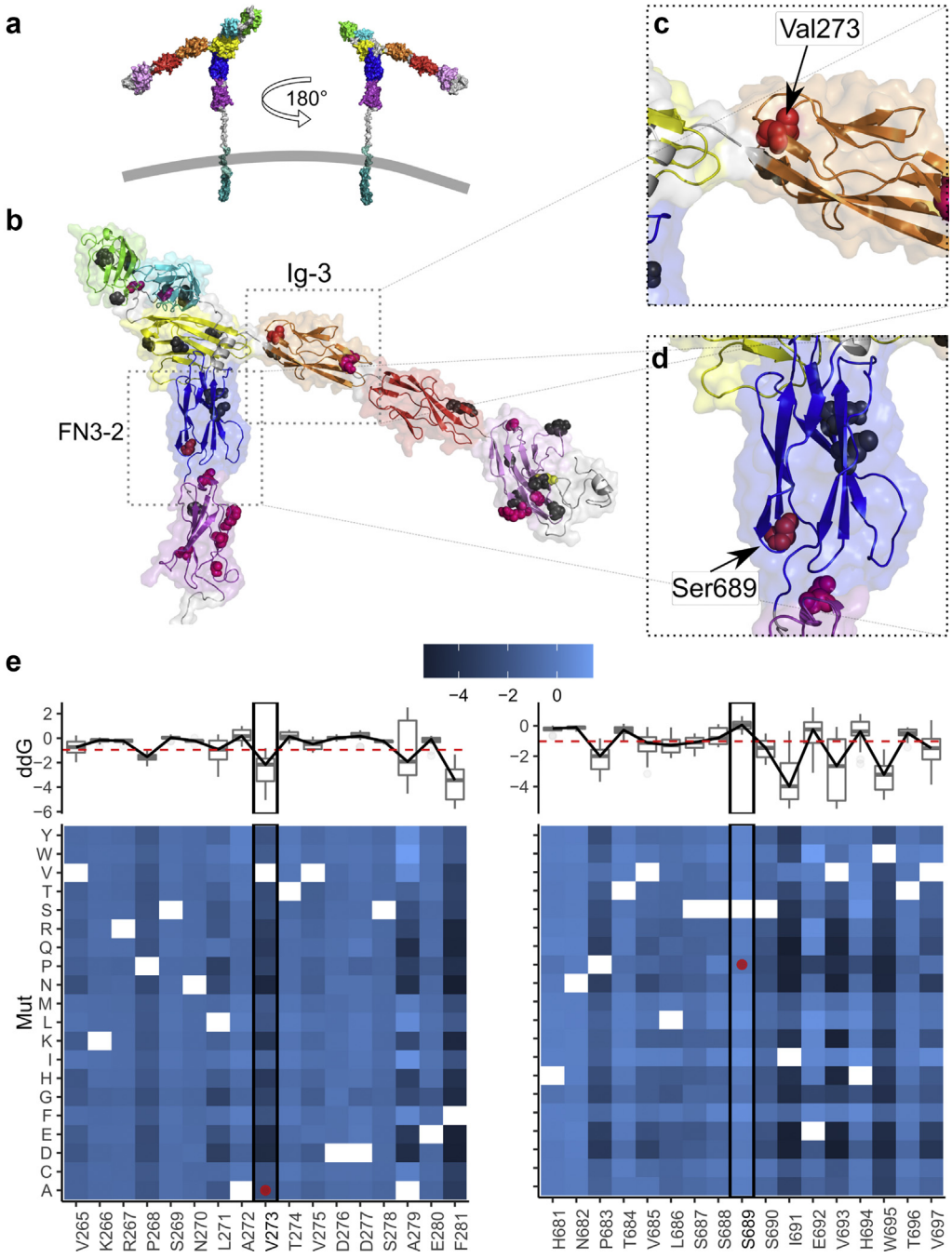

Figure 3 | Localization of missense variants in the ROBO1 3D-model. (**a**) Schematic overview of the ROBO1 model (N-terminal domain AAs 26-973) generated through the GalaxyTBM pipeline showing the 5 Ig-like C2-type and 3 fibronectin type III domains in surface representation (colored as in Figure 2a). The model is rotated by 180° on the *y*-axis on the right side. The helical transmembrane domain is anchored in a schematic cell membrane. (**b**) Zoom in with the same positioning as in the right side of (**a**) with transparent surface and protein backbone shown as cartoon. Position of missense variants identified in ID 1 (p.Val273; Ig-3 domain; red) and ID 4 (p.Ser689; FN3-2 domain; red) are presented as spheres. Missense variants in other ROBO orthologs associated with diseases are mapped onto the ROBO1 model and presented as colored spheres (ROBO2: pink; ROBO3: gray; ROBO4: yellow; compare Supplementary File S2 sheet "Related_variants"). (**c**) Zoom in showing that the c.818T>C, p.(Val273Ala) (ID 1) variant affects a surface loop in the Ig-3 domain. The variant is in close proximity to the mapped position of ROBO3 c.955G>A, p.(Glu319Lys),[35] one of the first variants described as pathogenic for familial horizontal gaze palsy with progressive scoliosis (MIM #607313). The Val273 AA is also in close proximity to the linker between Ig-3 and Ig-4. Both these domains have been implicated ROBO dimerization.[34] (**d**) Zoom in showing that the c.2065T>C, p.(Ser689Pro) variant affects a surface loop in the FN3-2 domain near the linker to FN3-3. The mapped ROBO2 variant c.2297A>G, p.(Asp766Gly), previously implicated in vesicoureteral reflux,[23] is located on the mirroring side FN3-3. The FN3-2 domain has been implicated in autoinhibition of ROBO signaling.[34] (**e**) Results of ddG analysis using DeepDDG[36] for the missense variants (±8 AAs) identified in individual ID 1 (Val273Ala, left panel, ddG = −1.984)and individual ID 4 (Ser689Pro, right panel, ddG = −0.552). The ddG values are color coded (dark blue more negative, light blue more positive) in the raster plot for each amino acid position (*x*-axis) and possible substitutions (*y*-axis) and the upper panel for each plot shows a connected (continued)

surface loop of the third Ig domain (Ig-3) in close proximity to the mapped position of *ROBO3* c.955G>A, p.(Glu319-Lys),[35] one of the first variants described as pathogenic for familial horizontal gaze palsy with progressive scoliosis (MIM #607313; Figure 3c). Furthermore, p.Val273 also localized in close proximity to the linker between Ig-3 and Ig-4, potentially interfering with homodimerization (Figure 3c).[34] Interestingly, the ENU-induced mouse model of *Robo1*$^{Ile270Thr/Ile270Thr}$ (NM_019413.2) also carries a missense mutation within Ig-3, which corresponds to p.(Ile309Thr) when translated to human *ROBO1* (NM_002941.3). Furthermore, we mapped p.(Ser689Pro) (ID 4) on the surface loop of the second FN3 domain (FN3-2) close to the linker to neighboring FN3-3 (Figure 3d). Of note, 1 previously reported *ROBO2* variant implicated in CAKUT phenotypes is thought to be positioned on the mirroring side of FN3-3, whereas FN3-2 itself has been linked to autoinhibition of ROBO signaling.[34] When calculating delta-delta-Gibbs free energy (ddG)[38,39] using DeepDDG,[36] a metric for predicting how single point mutations will affect protein stability, the Ig-3 change p.(Val273Ala) results in a negative ddG value meaning that these substitution is predicted to stabilize protein folding in a given way allowing less 3-dimensional flexibility (Figure 3e). On the contrary, calculation of ddG for p.(Ser689Pro) yields less negative values below recommended thresholds, implying different functional impacts on protein function such as interfering with autoinhibition of ROBO1 (Figure 3d and e).

Human ROBO1 expression during normal and disturbed nephrogenesis

To better characterize the role of ROBO1 in human nephrogenesis, we comparatively assessed ROBO1 expression in control and patient kidney samples at different gestational stages. Immunohistochemistry of endogenous ROBO1 in fetal control kidneys dating from 14 and 21 WG showed ROBO1 localization at the outer nephrogenic zone within comma-shaped bodies and S-shaped bodies supporting a role of ROBO1 in normal nephrogenesis (Figure 4a–d and Supplementary Figure S9). In contrast, the subcortical nephrogenic zone presented abolished in renal tissue from ID 8 at 22 WG accompanied by an absence of ROBO1 staining in severely dysplastic and cystic renal parenchyma (Figure 4e and f).

Mouse model

To assess the impact of *ROBO1* mutation on kidney development *in vivo*, we examined mice with the ENU-induced mutation *Robo1*$^{Ile270Thr/Ile270Thr}$ mentioned above.[12,28] The homozygous missense mutation in this mutant is located near the p.(Val273Ala) in Ig-3 when mapped to the human transcript (p.(Ile309Thr)). Using immunohistochemistry, we stained endogenous Robo1 in postnatal kidney sections from *Robo1* mutants and control littermates. Thereby, we found the complete absence of Robo1 expression in mutant kidneys, in contrast to the postnatal renal tubular expression observed in wild-type controls (Figure 5a–d and Supplementary Figure S10). Phenotypically, all newborn mutant mice (n = 5) displayed severely altered kidney architecture and genitourinary tract malformations compatible with CAKUT (Supplementary Table S1). Renal anomalies and hydroureter were first documented *in vivo* by the microCT scan of the mutant mice (Movie SV2). On necropsy, macroscopic renal phenotypes also included duplex or multiplex kidneys with cystic dysplasia and consecutive hydronephrosis (Figure 5e and f). Also observed were misplaced undescended gonads, both ovaries and testes, reminiscent of bilateral cryptorchidism reported in ID 3 (Figure 5). Histologically, proximal renal tubules were slightly dilated and microcystic (Figure 5g and h), whereas collecting ducts were highly cystic (Figure 5g and h). Comparable to observations in 5 of our patients (ID 1, ID 3, ID 4, ID 5, ID 9), *Robo1* mutant mice are known to exhibit congenital heart anomalies with double outlet right ventricle, atrioventricular septal defects, and ventricular septal defects as previously reported.[12] A similar analogy was observed for dysmorphic facial features, which had both been found in *Robo1* mutant mice and 8 of 9 patients (ID 2, ID 3, ID 4, ID 5, ID 6, ID 7, ID 8, ID 9).[12] As renal cystic dilation and extrarenal manifestations (e.g., heart anomalies) were reminiscent of ciliopathy phenotypes, we compared primary cilia protruding from collecting ducts and ureteric bud tips in control versus *Robo1* mutant animals. Ciliary morphology and abundance, however, was overall unaffected on staining with acetylated tubulin in immunofluorescent microscopy (Figure 5i–l).

DISCUSSION

We describe 6 unrelated individuals and 2 fetal cases from 1 family with CAKUT phenotypes and biallelic *ROBO1* variants. We further provide *in silico* and human protein expression data supporting the functional impact of these variants on ROBO1 and *in vivo* recapitulation of the observed human phenotypes in a previously reported mouse model. On the basis of these data, we here propose biallelic *ROBO1* variants as causing syndromic, but viable CAKUT phenotypes in humans. *ROBO1* has been a credible candidate gene for human CAKUT, at least since the report of a family with repetitive fetal demise, renal agenesis, and concomitant *ROBO1* loss-of-function[19] and perhaps as far back as 2007 when its paralog *ROBO2* was associated with CAKUT.[22]

Figure 3 | (continued) boxplot for all possible substitutions at the position. Amino acid positions affected by the 2 missense variants are highlighted by a black box and marked by a red dot. ddG values are based on the PDB structures 5o5g (Ig-3 domain) and 4hlj (FN3-2 domain). The result for p.(Val273Ala) indicates that these substitutions stabilize the protein and possibly reduces folding flexibility. p.(Ser689Pro) in contrast is below the recommended thresholds (<−1 or >+1) and thus likely has different effects on the protein function like intramolecular interaction (compare D; ddG values provides in Supplementary File S2).

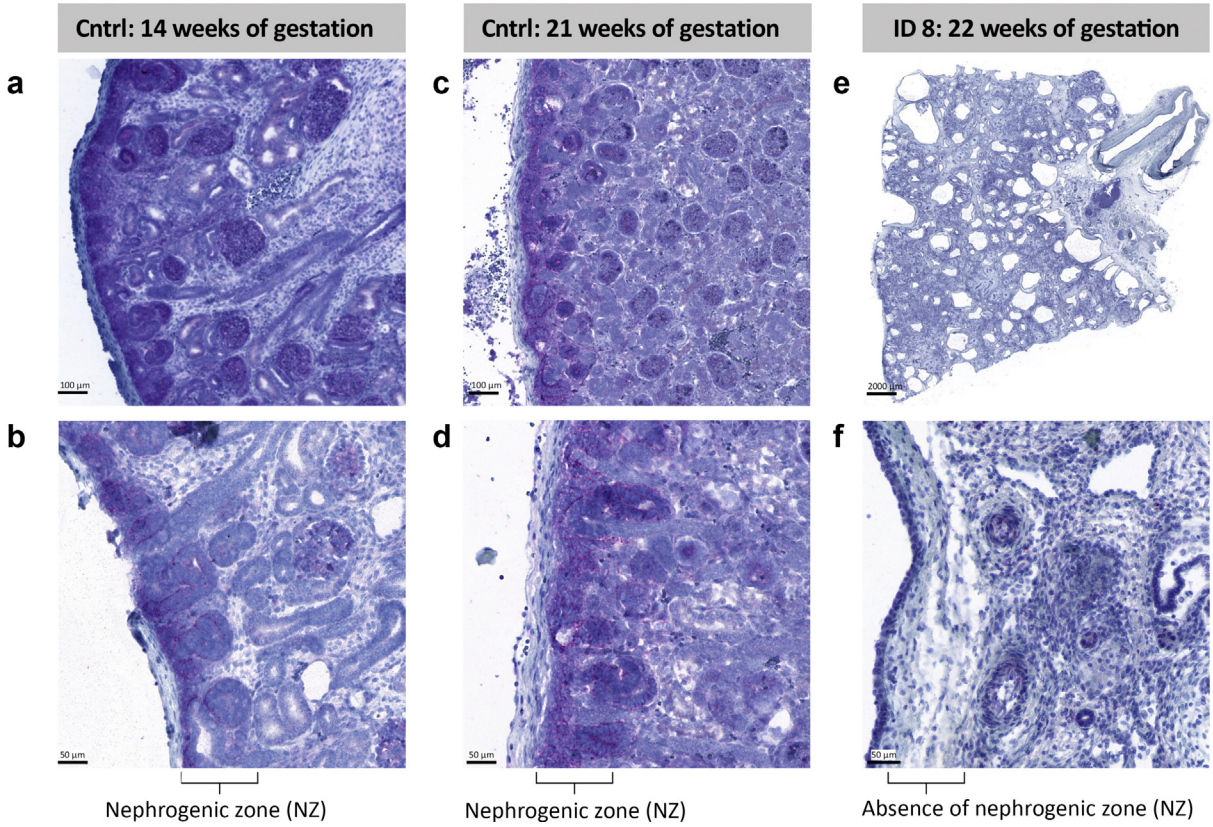

Figure 4 | Human ROBO1 expression in normal and disturbed nephrogenesis. (**a**) ROBO1 immunohistochemistry in fetal kidneys from independent controls (Cntrl) at 14 and 21 weeks of gestation (**a–d**) and from patient ID 8 at 22 weeks of gestation (**e,f**). Of note, while ROBO1 expression is most abundant in the nephrogenic zone (NZ) of both control samples, NZ appears abolished in the patient sample accompanied by an absence of ROBO1 positive staining. Instead, the renal parenchyma is characterized by marked cystic tubular dilation with a reduced number of glomeruli in ID 8. Bar = 100 µm in the upper panel and 50 µm in the lower panel (except 2000 µm in **e**). To optimize viewing of this image, please see the online version of this article at www.kidney-international.org.

However, additional *ROBO1* variant families have not been reported since, and it has been unclear whether biallelic *ROBO1* alteration is compatible with life. Meanwhile, heterozygous variants have been associated with congenital heart disease and neurodevelopmental conditions. Activation of the Slit-Robo pathway has been implicated in neuronal and cardiac development; however, its major players were also found to be expressed in murine embryonic kidneys, notably in the metanephric mesenchyme (Robo1/Slit1) and S-shaped bodies (Robo2, Slit2, and Slit3),[40] a finding that we were able to confirm for ROBO1, which we found to be expressed in the outer nephrogenic zone of human fetal control kidneys at 14 and 21 WG. Consequently, both ROBO2 and SLIT2, as well as its partner SRGAP1, have been implicated in human and murine CAKUT.[22-24,41–43] In contrast to our observations in *ROBO1*, VUR associated with *ROBO2* was observed on monoallelic variation and dominant inheritance with incomplete penetrance (MIM #610878). Similarly, identified CAKUT-associated variants in *SLIT2* and *SRGAP1* were reported heterozygous with incomplete penetrance.[24] The fact that identified *ROBO2/SLIT2/SRGAP2* variants were also present in healthy carriers raised controversies about their pathogenic impact and prompted some authors to suggest their classification as risk variants instead of disease-causing variants.[44] Herein, we present data to support an alternative hypothesis: although previous studies also claimed monoallelic *ROBO1* mutations to be associated with cardiac phenotypes, heterozygous parents in our study were clinically unaffected, which we propose may be due to incomplete penetrance and gene dosage effects conferred by distinct variants in the *ROBO1* locus.[7] According to our data, renal involvement was only present on genetic alteration of both alleles. We therefore propose *ROBO1*-associated CAKUT to represent a recessive disease.

Similar to recessive ciliopathies, both mouse and human phenotypes included cystic tubular dilation with extrarenal anomalies affecting the heart, the brain, and the eye. In addition, ROBO1 and ROBO2 were previously shown to locate to primary cilia in interneurons.[45] Our preliminary investigations yielded normal ciliogenesis in renal collecting ducts and ureteric bud tips in *Robo1* mutant mice. However, disturbances of ciliary signaling cannot be excluded by these data.

Mechanistically, ROBO1 was shown to both homodimerize and heterodimerize with ROBO2[46] as well as with SLIT ligands 1/2/3 and SRGAP1/2.[46] Although identified

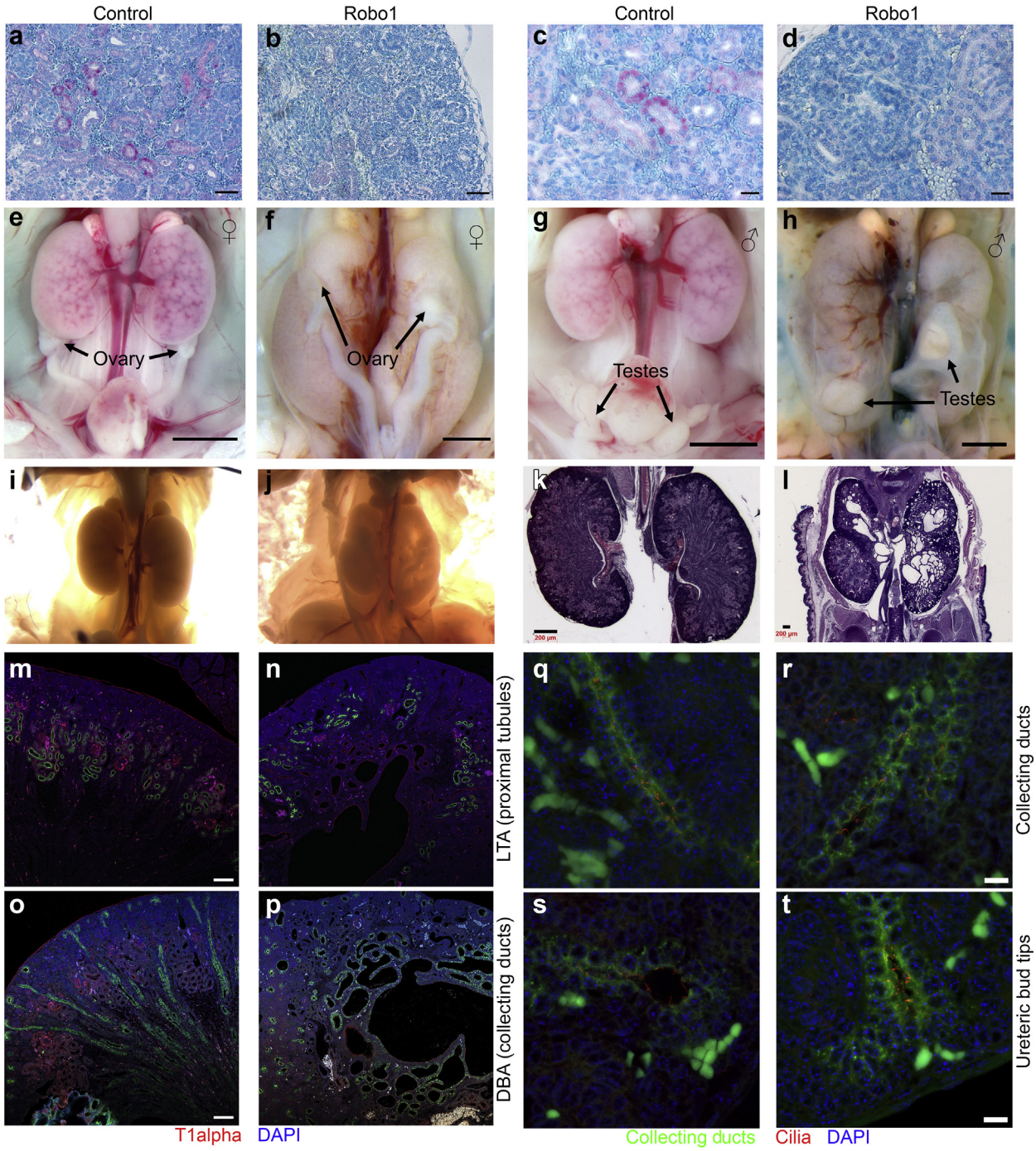

Figure 5 | CAKUT phenotypes in *Robo1* mutant mouse. (**a–d**) Immunohistochemistry of Robo1 showing the absence of Robo1 expression in *Robo1* mutant mice versus postnatal tubular expression in control littermates. (**e–j**) Necropsy photos of control (**e,g,i**) and *Robo1* mutant animals (**f,h,j**). Apart from multiple kidneys with associated ureters on each side (**f,h,j**), *Robo1* mutant mice display misplaced ovaries in females (**f**) and maldescended testes in males (**h**). (**k,l**) Hematoxylin and eosin–stained sections of control (**k**) and *Robo1* mutant (**l**) kidneys. The Robo1 mutants have multiple kidneys within the same capsule. The kidneys show extensive large medullary cysts and hydrophrosis with smaller cysts or tubule dilations in the cortex. Note that the images are at different magnifications but the bars = 200 μm. (**m,n**) Control and *Robo1* mutant kidneys labeled with the proximal tubule marker Lotus tetragonolobus agglutinin (LTA, green), the glomerular marker T1alpha (red), and a nuclear marker (4′,6-diamidino-2-phenylindole [DAPI], blue). Proximal tubules show only minimal cystic dilation. Bar = 100 μm. (**o,p**) Control and *Robo1* mutant kidneys labeled with the collecting duct marker Dolichos biflorus agglutinin (DBA, green), the glomerular marker T1alpha (red), and a nuclear marker (DAPI, blue). Collecting ducts are highly cystic. Bar = 100 μm. (**q–t**) Control and *Robo1* mutant kidneys labeled with the collecting duct marker DBA (green), the ciliary marker 6-11B-1 (red), and a nuclear marker (DAPI, blue). Collecting ducts are highly cystic. Q and R represent examples of collecting ducts, and S and T are ureteric bud tips. Bar = 10 μm. To optimize viewing of this image, please see the online version of this article at www.kidney-international.org.

truncating and canonical splice site variants are mainly thought to result in reduced RNA and protein stability, 4 of them (c.687C>G, p.(Tyr229*), c.850G>T, p.(Glu284*), c.1198C>T, p.(Gln400*), and c.1342+1G>A) may even abrogate the protein-protein interaction due to loss of prominent functional domains, such as Ig-like and FN3, critical domains to which identified missense variants were mapped by homology modeling. Although the first and second Ig-like domain were shown to mediate Slit binding,[47] p.(Val273Ala) locates to the third Ig-like domain, known to be crucial for homodimerization. The second missense variant, p.(Ser689Pro), was mapped to the second of 3 FN3 domains located close to the transmembrane region. This particular FN3 domain was shown to be important for ROBO2 autoinhibition by shielding an important ROBO1/2 dimerization interface required for signaling. This suggests that the deduced Serine to Proline change may interfere with ROBO autoinhibition to influence Slit-Robo signaling.

In our study, the 2 individuals without severe intellectual impairment (ID 1 and ID 4) carried truncating variants in combination with likely hypomorphic missense variants, probably attenuating the phenotype and making viability more likely. Observed phenotypes were remarkably heterogeneous in the cases reported, consistent with variable expressivity representing a hallmark of CAKUT. Unlike in *Robo1* mutant mice, none of our patients showed multiplex kidneys. Instead, 5 patients exhibited unilateral or bilateral renal agenesis pointing to differences of ROBO1 function during murine and human nephrogenesis. The 3 fetal sibs illustrate the large intrafamilial variability in *ROBO1*-associated CAKUT, ranging from bilateral kidney agenesis in ID 7 to unilateral agenesis and kidney dysplasia in ID 8, whereas ID 9 presented with normal kidneys but severe extrarenal manifestations incompatible with life. This extreme phenotypic variability has been reported in 1 family before.[19] Nevertheless, in live-born individuals overall kidney disease seemed relatively mild and end-stage kidney disease was only reached at 44 years of age in the only adult patient (ID 1) identified, probably postponed by timely VUR diagnosis and subsequent surgical correction, which may have helped to preserve renal function for decades. CKD, however, appears to be a variable manifestation of a broad phenotypic spectrum in *ROBO1*-associated disease. In ID 2 and ID 3, both carrying homozygous splice site variants, neurodevelopmental defects dominated the clinical appearance with characteristic craniofacial features and a mirror hand movement phenotype, implying a role of ROBO1 in axon guidance for spinal interneurons. Axon guidance defects are illustrated by cerebral studies in the 3 fetal cases (ID 7, ID 8, ID 9), showing the absence of pyramidal tracks in all of them and partial agenesis of the corpus callosum in 2 of them. Strikingly, eye and heart anomalies in terms of strabismus and cardiac valve defects were present in the majority (5 of 9) of patients reported (no data in ID 4 and ID 6 available). Regarding pituitary malformations, we also observed variable expressivity. The missing "bright spot" at the posterior pituitary gland in ID 1 was asymptomatic and remained without clinical implications as endocrine laboratory testing revealed no further abnormalities.

The expression of *ROBO1* in multiple tissues may explain vastly heterogeneous organ involvement and their variable presentation may depend on allelic combinations and gene dosage effects, as recently demonstrated for *TBX6*, a gene associated with similar clinical heterogeneity in syndromic CAKUT.[7] Furthermore, genetic and epigenetic modifiers as well as missed intronic or regulatory germline variants modulating the phenotype on an individual basis cannot be ruled out at this point. Therefore, suspected *ROBO1*-associated disease requires extensive screening for eye, heart, central nervous system, gonad, and kidney involvement in order to capture the full clinical picture.

In conclusion, we propose biallelic *ROBO1* variants to represent a bona fide cause of viable syndromic CAKUT phenotypes. As the diagnostic yield of genetic analysis is still insufficient in patients suffering from CAKUT, generating genetic evidence for putative gene-disease associations is urgently required in order to increase genetic testing efficiency and facilitate consultation. Moreover, noncoding contributing variants at the *ROBO1* and *ROBO2* loci should be considered in CAKUT penetrance of copy number variations including these loci. Therefore, we propose *ROBO1* to become part of routine genetic evaluation in all individuals affected by CAKUT ranging from nonviable fetus to live-born newborns to adults with previously missed genetic diagnostics.

DISCLOSURE

Baylor College of Medicine and Miraca Holdings have formed a joint venture with shared ownership and governance of the Baylor Genetics, which performs clinical microarray analysis and other genomic studies (exome sequencing, whole genome sequencing) for patient/family care. JRL serves on the Scientific Advisory Board of the Baylor Genetics. He has stock ownership in 23andMe, is a paid consultant for Regeneron Pharmaceuticals, and is a coinventor on multiple United States and European patents related to molecular diagnostics for inherited neuropathies, eye diseases, and bacterial genomic fingerprinting. CB is the Medical and Managing Director of Medizinische Genetik Mainz and Limbach Genetics.

DATA STATEMENT

The panel sequencing design for ID 1 is provided in Supplementary File S1 and all raw *in silico* data are provided in Supplementary File S2, which has been submitted to Zenodo together with the Supplementary Movies S1A/B and S2 (https://doi.org/10.5281/zenodo.5716336). All protein models have been submitted to Zenodo (https://doi.org/10.5281/zenodo.4546112). Further original data regarding the mouse model are available from the authors on reasonable request.

ACKNOWLEDGMENTS

We thank Dr. S. Stoebe (University Medical Center Leipzig) for providing cardiac imaging data.

This work was supported in part by the German Research Foundation (Deutsche Forschungsgemeinschaft [DFG]—HA 6908/3-1 to JH), the Else Kroener Fresenius Foundation (EKES—to JH), US

National Institutes of Health, National Human Genome Research Institute (NHGRI)/National Heart, Lung, and Blood Institute (NHLBI) UM1 HG006542 to the Baylor Hopkins Center for Mendelian Genomics (JRL) and the National Institute of Neurological Disorders and Stroke (R35 NS105078 to JRL). JEP was supported by NHGRI K08 HG008986. BP was supported by the German Research Foundation (DFG) grant PO2366/2-1. CB receives support from the Deutsche Forschungsgemeinschaft (DFG) (BE 3910/8-1, BE 3910/9-1, and Project-ID 431984000 – Collaborative Research Center SFB 1453) and the Federal Ministry of Education and Research (BMBF, 01GM1903I and 01GM1903G). SD receives a grant for the Initiative on Rare and Undiagnosed Diseases in Pediatrics (no. 18gk0110012h0101) from the Japan Agency for Medical Research and Development (AMED), Tokyo, Japan. LRC was supported by the Dutch Kidney Foundation (18OKG19 to AMvE). Several authors of this publication are members of the European Reference Network for Rare Kidney Diseases (ERKNet)—Project ID No. 739532. This research was further made possible through access to the data and findings generated by the 100,000 Genomes Project. The 100,000 Genomes Project is managed by Genomics England Limited (a wholly owned company of the Department of Health and Social Care). The 100,000 Genomes Project is funded by the National Institute for Health Research and NHS England. The Wellcome Trust, Cancer Research UK, and the Medical Research Council have also funded research infrastructure. The 100,000 Genomes Project uses data provided by patients and collected by the National Health Service as part of their care and support. The diagnosis of ID 7 was made possible through access to the data generated by the 2025 French Genomic Medicine Initiative.

AUTHOR CONTRIBUTIONS

JM, JH, and BP conceived the study; JM, ME, JAH, BT, TSh, GA, SD, AP, TWe, AAS, JH, FP, HF, and LD gathered clinical data; LRC and AMvE contributed in identifying further affected individuals; CB, TWa, SD, TSm, DP, TM, ZCA, JEP, SS, SP, JB, JRL, and TA-B performed genetic analysis; BP, RS, and EH performed RNA analysis; BP and AAM performed *in silico* analysis; GJP, GCG, and CWL contributed murine model analysis; CH and AKH performed antibody validation and immunohistochemistry; AAS, ZCA, JEP, and JRL gave highly appreciated advice for this study and edited the manuscript; JM, ME, BP, JH, and FP wrote the manuscript. All authors read, edited, and accepted the final manuscript version.

SUPPLEMENTARY MATERIAL

Supplementary File (Word)

Figure S1. Multiple-sequence alignment (MSA) and branching diagram of human ROBO protein Ig domains.
Figure S2. Multiple-sequence alignment (MSA) and branching diagram of human ROBO protein fibronectin type III (FN3) domains.
Figure S3. Multiple-sequence alignment (MSA) of ROBO protein Ig domain orthologs.
Figure S4. Branching diagram of ROBO protein Ig domain orthologs.
Figure S5. Multiple-sequence alignment (MSA) of ROBO protein fibronectin type III (FN3) domain orthologs.
Figure S6. Branching diagram of ROBO protein fibronectin type III (FN3) domain orthologs.
Figure S7. Localization of missense variants in ROBO1 tetramer.
Figure S8. Comparison of the GalaxyTBM model with published ROBO1/2 models.
Figure S9. Human fetal control kidney sections (14 weeks of gestation).
Figure S10. Validation of the ROBO1 antibody *in vitro*.
Table S1. Kidney and gonad defects in *Robo1* mutant mouse line (n = 5).

Supplementary File S1 (Excel)

File S1. Four hundred twenty-six genes (chronic kidney disease [CKD]–panel content—ID 1). Excel file containing the 2 sheets "summary" and "panel_content." The summary file explains the content of the other sheet in detail. Supplementary File S1 has been submitted to Zenodo (https://doi.org/10.5281/zenodo.5716336).

Supplementary File S2 (Excel)

File S2. Variants and domains. Excel file containing the 11 sheets "summary," "Domains," "ROBO1_variants," "ROBO1_allMissense," "Related_proteins," "Related_variants," "ROBO1MappingTable," "ROBO2MappingTable," "5o5g_Ig1ToIg4_DDG," "5o5i_Ig5_DDG," and "4hlj_FN32ToFN33_DDG." These tables contain all *in silico* data for variants used in the figures. The summary file explains the content of the other sheet in detail. Supplementary File S2 has been submitted to Zenodo (https://doi.org/10.5281/zenodo.5716336).

Supplementary File (Movie SV1A)

Movie SV1A. Transthoracic apical long axis view with a mild-to-moderate mitral valve regurgitation (Vivid E9, GE Vingmed Ultrasound, Horten, Norway).

Supplementary File (Movie SV1B)

Movie SV1B. Anterior-directed jet formation due to primary P2-mitral valve prolapse (Vivid E9, GE Vingmed Ultrasound, Horten, Norway). Supplementary Video SV1 has been submitted to Zenodo (https://doi.org/10.5281/zenodo.5716336).

Supplementary File (Movie SV2)

Movie SV2. Newborn mutant mice displayed severely altered kidney architecture and urinary tract malformations compatible with CAKUT. Renal anomalies and hydroureter were first documented *in vivo* by the microCT scan of the mutant mice. Supplementary Video SV2 has been submitted to Zenodo (https://doi.org/10.5281/zenodo.5716336).

REFERENCES

1. Chesnaye N, Bonthuis M, Schaefer F, et al. Demographics of paediatric renal replacement therapy in Europe: a report of the ESPN/ERA-EDTA registry. *Pediatr Nephrol*. 2014;29:2403–2410.
2. Ottlewski I, Münch J, Wagner T, et al. Value of renal gene panel diagnostics in adults waiting for kidney transplantation due to undetermined end-stage renal disease. *Kidney Int*. 2019;96:222–230.
3. Sanna-Cherchi S, Ravani P, Corbani V, et al. Renal outcome in patients with congenital anomalies of the kidney and urinary tract. *Kidney Int*. 2009;76:528–533.
4. Knoers NVAM, Renkema KY. The genomic landscape of CAKUT; you gain some, you lose some. *Kidney Int*. 2019;96:267–269.
5. van der Ven AT, Vivante A, Hildebrandt F. Novel insights into the pathogenesis of monogenic congenital anomalies of the kidney and urinary tract. *J Am Soc Nephrol*. 2018;29:36–50.
6. Verbitsky M, Westland R, Perez A, et al. The copy number variation landscape of congenital anomalies of the kidney and urinary tract. *Nat Genet*. 2019;51:117–127.
7. Yang N, Wu N, Dong S, et al. Human and mouse studies establish TBX6 in Mendelian CAKUT and as a potential driver of kidney defects associated with the 16p11.2 microdeletion syndrome. *Kidney Int*. 2020;98:1020–1030.
8. Sanna-Cherchi S, Westland R, Ghiggeri GM, Gharavi AG. Genetic basis of human congenital anomalies of the kidney and urinary tract. *J Clin Invest*. 2018;128:4–15.
9. Nicolaou N, Renkema KY, Bongers EMHF, et al. Genetic, environmental, and epigenetic factors involved in CAKUT. *Nat Rev Nephrol*. 2015;11:720–731.
10. Bisiak F, McCarthy AA. Structure and function of roundabout receptors. *Subcell Biochem*. 2019;93:291–319.
11. Kidd T, Brose K, Mitchell KJ, et al. Roundabout controls axon crossing of the CNS midline and defines a novel subfamily of evolutionarily conserved guidance receptors. *Cell*. 1998;92:205–215.
12. Kruszka P, Tanpaiboon P, Neas K, et al. Loss of function in ROBO1 is associated with tetralogy of Fallot and septal defects. *J Med Genet*. 2017;54:825–829.
13. Rafipay A, Dun X-P, Parkinson DB, et al. Knockdown of slit signaling during limb development leads to a reduction in humerus length. *Dev Dyn*. 2021;250:1340–1357.

14. Liu J, Hou W, Guan T, et al. Slit2/Robo1 signaling is involved in angiogenesis of glomerular endothelial cells exposed to a diabetic-like environment. *Angiogenesis*. 2018;21:237–249.
15. Rama N, Dubrac A, Mathivet T, et al. Slit2 signaling through Robo1 and Robo2 is required for retinal neovascularization. *Nat Med*. 2015;21:483–491.
16. Bashamboo A, Bignon-Topalovic J, Moussi N, et al. Mutations in the human ROBO1 gene in pituitary stalk interruption syndrome. *J Clin Endocrinol Metab*. 2017;102:2401–2406.
17. Liu Z, Chen X. A novel missense mutation in human Receptor Roundabout-1 (ROBO1) gene associated with pituitary stalk interruption syndrome. *J Clin Res Pediatr Endocrinol*. 2020;12:212–217.
18. Calloni SF, Cohen JS, Meoded A, et al. Compound heterozygous variants in ROBO1 cause a neurodevelopmental disorder with absence of transverse pontine fibers and thinning of the anterior commissure and corpus callosum. *Pediatr Neurol*. 2017;70:70–74.
19. Rasmussen M, Sunde L, Nielsen ML, et al. Targeted gene sequencing and whole-exome sequencing in autopsied fetuses with prenatally diagnosed kidney anomalies. *Clin Genet*. 2018;93:860–869.
20. Dateki S, Watanabe S, Mishima H, et al. A homozygous splice site ROBO1 mutation in a patient with a novel syndrome with combined pituitary hormone deficiency. *J Hum Genet*. 2019;64:341–346.
21. Nicolaou N, Pulit SL, Nijman IJ, et al. Prioritization and burden analysis of rare variants in 208 candidate genes suggest they do not play a major role in CAKUT. *Kidney Int*. 2016;89:476–486.
22. Lu W, van Eerde AM, Fan X, et al. Disruption of ROBO2 is associated with urinary tract anomalies and confers risk of vesicoureteral reflux. *Am J Hum Genet*. 2007;80:616–632.
23. Bertoli-Avella AM, Conte ML, Punzo F, et al. ROBO2 gene variants are associated with familial vesicoureteral reflux. *J Am Soc Nephrol*. 2008;19:825–831.
24. Hwang D-Y, Kohl S, Fan X, et al. Mutations of the SLIT2-ROBO2 pathway genes SLIT2 and SRGAP1 confer risk for congenital anomalies of the kidney and urinary tract. *Hum Genet*. 2015;134:905–916.
25. Sobreira N, Schiettecatte F, Valle D, Hamosh A. GeneMatcher: a matching tool for connecting investigators with an interest in the same gene. *Hum Mutat*. 2015;36:928–930.
26. Ko J, Park H, Seok C. GalaxyTBM: Template-based modeling by building a reliable core and refining unreliable local regions. *BMC Bioinformatics*. 2012;13:198.
27. Ko J, Park H, Heo L, Seok C. GalaxyWEB server for protein structure prediction and refinement. *Nucleic Acids Res*. 2012;40:W294–W297.
28. San Agustin JT, Klena N, Granath K, et al. Genetic link between renal birth defects and congenital heart disease. *Nat Commun*. 2016;7:11103.
29. Coban-Akdemir Z, White JJ, Song X, et al. Identifying genes whose mutant transcripts cause dominant disease traits by potential gain-of-function alleles. *Am J Hum Genet*. 2018;103:171–187.
30. Rentzsch P, Witten D, Cooper GM, et al. CADD: predicting the deleteriousness of variants throughout the human genome. *Nucleic Acids Res*. 2019;47:D886–D894.
31. Karczewski KJ, Francioli LC, Tiao G, et al. The mutational constraint spectrum quantified from variation in 141,456 humans. *Nature*. 2020;581:434–443.
32. Lupski JR, Belmont JW, Boerwinkle E, Gibbs RA. Clan genomics and the complex architecture of human disease. *Cell*. 2011;147:32–43.
33. Gonzaga-Jauregui C, Yesil G, Nistala H, et al. Functional biology of the Steel syndrome founder allele and evidence for clan genomics derivation of COL27A1 pathogenic alleles worldwide. *Eur J Hum Genet*. 2020;28:1243–1264.
34. Barak R, Yom-Tov G, Guez-Haddad J, et al. Structural principles in Robo activation and auto-inhibition. *Cell*. 2019;177:272–285.e16.
35. Jen JC, Chan W-M, Bosley TM, et al. Mutations in a human ROBO gene disrupt hindbrain axon pathway crossing and morphogenesis. *Science*. 2004;304:1509–1513.
36. Cao H, Wang J, He L, et al. DeepDDG: predicting the stability change of protein point mutations using neural networks. *J Chem Inf Model*. 2019;59:1508–1514.
37. Aleksandrova N, Gutsche I, Kandiah E, et al. Robo1 forms a compact dimer-of-dimers assembly. *Structure*. 2018;26:320–328.e4.
38. Kellogg EH, Leaver-Fay A, Baker D. Role of conformational sampling in computing mutation-induced changes in protein structure and stability. *Proteins*. 2011;79:830–838.
39. Park H, Bradley P, Greisen P, et al. Simultaneous optimization of biomolecular energy functions on features from small molecules and macromolecules. *J Chem Theory Comput*. 2016;12:6201–6212.
40. Piper M, Georgas K, Yamada T, Little M. Expression of the vertebrate Slit gene family and their putative receptors, the Robo genes, in the developing murine kidney. *Mech Dev*. 2000;94:213–217.
41. Liu J, Sun L, Shen Q, et al. New congenital anomalies of the kidney and urinary tract and outcomes in Robo2 mutant mice with the inserted piggyBac transposon. *BMC Nephrol*. 2016;17:98.
42. Mitsioni AG, Siomou E, Bouba I, et al. ROBO2 gene variants in children with primary nonsyndromic vesicoureteral reflux with or without renal hypoplasia/dysplasia. *Pediatr Res*. 2016;80:72–76.
43. Zu S, Bartik Z, Zhao S, et al. Mutations in the ROBO2 and SLIT2 genes are rare causes of familial vesico-ureteral reflux. *Pediatr Nephrol*. 2009;24:1501–1508.
44. Dobson MG, Darlow JM, Hunziker M, et al. Heterozygous non-synonymous ROBO2 variants are unlikely to be sufficient to cause familial vesicoureteric reflux. *Kidney Int*. 2013;84:327–337.
45. Higginbotham H, Eom T-Y, Mariani LE, et al. Arl13b in primary cilia regulates the migration and placement of interneurons in the developing cerebral cortex. *Dev Cell*. 2012;23:925–938.
46. Hivert B, Liu Z, Chuang C-Y, et al. Robo1 and Robo2 are homophilic binding molecules that promote axonal growth. *Mol Cell Neurosci*. 2002;21:534–545.
47. Morlot C, Thielens NM, Ravelli RBG, et al. Structural insights into the Slit-Robo complex. *Proc Natl Acad Sci U S A*. 2007;104:14923–14928.